Microstructural investigation of snow metamorphism with the SnowMicroPenetrometer

Bruno POIRIER

Supervisors :
Pascal HAGENMULLER and Isabel PEINKE

B. Eng. Internship Final Report

Météo - France - CNRS\CNRM\CEN, Grenoble

January 15th to May 18th 2018

Abstract

In this study we assess the SnowMicroPenetrometer's (SMP) capacity to characterize the evolution through time of the microstructure of two snow samples: one undergoing a strong temperature gradient and another that is kept isothermal. Penetration resistance, density and specific surface area are measured daily for fifteen days to track snow evolution. SMP force-distance signals, being challenging to interpret as is, are analyzed aided from different models: the Poisson shot noise, the continuum cavity expansion model (CEM) and a density model. The latter two bring little information regarding microstructure evolution whereas the Poisson shot noise increases our understanding of certain phenomena. Indeed it explains the poor cohesion of faceted snow to be caused by a lesser amount of ice bonds and not to a decreasing individual strength of the bonds, which is in fact increasing. The density model, after calibration on both samples, yields results resembling the average of both samples. As for the CEM, it yields a constant modulus of elasticity for snow when density increases which is contradictory to results found in literature.

Contents

1 Introduction

Snow undergoes structural metamorphism, a phenomenon whose rate and nature are strongly dependent of the temperature difference between the bottom and top of the snow pack as well as its thickness, known as temperature gradient. Metamorphism can lead to either a greater cohesion amongst snow grains, which will stabilize the snow pack, or a weaker one. A snow pack layer consisting of poorly cohesive grains can collapse if triggered by external stress such as a heavy snowfall or a skier making a turn for instance, leading to an avalanche.

Structural properties of the snow pack have been measured with cone penetration tests since the 1930's with the Ramsonde test, and more recently with the SnowMicroPenetrometer (SMP).

The SMP is a high-resolution penetrometer that measures snow hardness through penetration resistance [Schneebeli and Johnson, 1998]. Its conical indenter is mounted on a piezoelectric sensor able to pick up small-scale strain, such as snow grain fractures, which is then converted to a force signal. Each snow sample or snow pack is characterized by a unique force-distance signal across its depth depending on several variables such as grain type or density [Pielmeier and Schneebeli, 2003].

Much work was done in the past in regards of processing SMP signals: by describing the penetration force as a Poisson shot noise process, Löwe and van Herwijnen [2011] derive expressions of micromechanical parameters from statistical characteristics of the SMP force signal. These grain-scale parameters are the individual rupture strength f_0, deflection at rupture δ and the event intensity λ. Later, Ruiz et al. [2017] proposed and tested a cavity-expansion-based penetration model (CEM) which estimated bulk mechanical properties such as yield stress σ_{mac} and elastic modulus E_{mac} from radial static equilibrium equations. This method was then compared to Löwe and van Herwijnen [2011]'s by inferring a macroscopic yield stress and an elastic modulus based on Johnson and Schneebeli [1999] and Marshall and Johnson [2009]'s work. The outcome of this comparison showed that the CEM was effective in predicting the elastic modulus for all snow densities when compared to experimental data from Mellor [1974], whereas the shot noise model failed at higher densities.

Proksch et al. [2015] further investigated the SMP's adequacy for estimation of snow density and proposed a regression model which computes density based on statistics of the force signal aided from experimental density values from CT-scans. A similar model for SSA estimation was also proposed.

The purpose of this study is to assess the SMP's capacity to assess the evolution of snow microstructure with metamorphism in a quantitative manner based on computed micro- and macromechanical parameters from existing statistical and solid mechanics models. Bulk mechanical properties from both CEM and a modified version of the shot noise model are computed. The latter will differ in a way that its parameter λ will become depth-dependent and different window sizes will be used. A comparison of the density model and experimental data will also be done in this study.

This study will be conducted on snow samples undergoing both weak and strong temperature gradients leading to distinct grain metamorphism. The effects of gradient metamorphism on mechanical properties can assumedly be isolated from sintering effects if measurements are performed after sintering ceases.

2 Experimental Method

2.1 Temperature gradient and isothermal apparatus

In order to simulate a snow pack undergoing a temperature gradient as it does in nature, an apparatus (Figure 2) from a former experiment was employed. This apparatus features two hollow copper plates allowing cooling fluid to flow within and hence regulate temperature when hooked to cryostats. The plates are hooked up to two separate cryostats. The upper plate is removable and allows sieving directly inside the apparatus, minimizing snow handling. The sample dimensions are of 50 cm wide, 100 cm long and 22 cm thick. Plate temperatures are set to: $-7\,^{\circ}\mathrm{C}$ for upper plate and $-1\,^{\circ}\mathrm{C}$ for lower plate, yielding a gradient of $27\,^{\circ}\mathrm{C/m}$ which is categorized as a strong gradient and is expected to lead to fully faceted snow in about three weeks' time based on literature [Calonne et al., 2014]. The apparatus is located in a cold room at $-4\,^{\circ}\mathrm{C}$ and about 50% relative humidity. Plates are equipped with eight $PT-100$ temperature sensors located on their inner surface to monitor temperature trend throughout the experiment.

Similarly, a reference snow sample of equal volume was kept in an insulated container and underwent no temperature gradient (Figure 5b). Four temperature sensors inside the container monitored temperature variations.

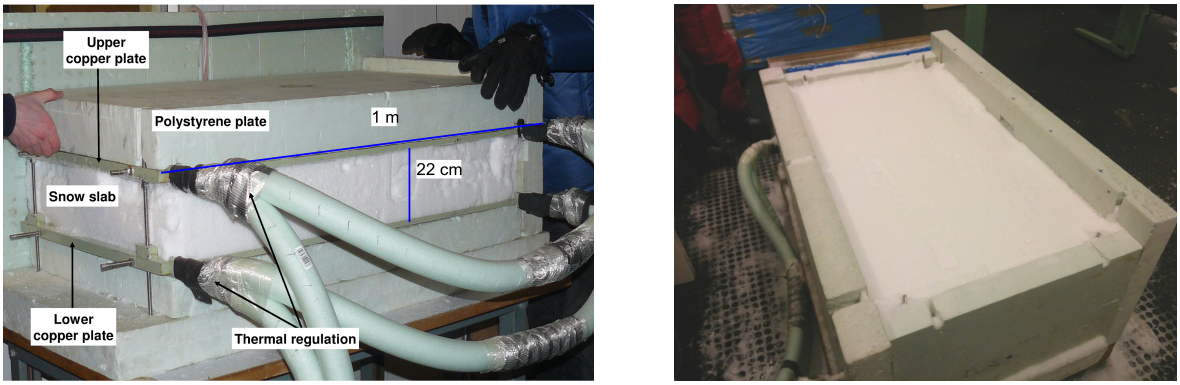

(a) With polystyrene side walls removed to show snow sample and copper plates.

(b) Seen from above with upper plate removed to perform SMP measurement.

Figure 2: In-house manufactured temperature gradient apparatus.

2.2 Snow sampling and preparation

About 1 m^3 of fresh snow of grain type PP/DF [Fierz et al., 2009] was collected from Col d'Ornon (1367 m) in the French Alps at $-4\,^{\circ}\mathrm{C}$ and 100 $\mathrm{kg/m}^3$ in windless and cloudy conditions on March 5th 2018. It was then transported by truck for an hour in insulated containers. Snow temperature was kept constant during the trip. The sampling snow was then stored in a cold room for a week at $-20\,^{\circ}\mathrm{C}$. The snow was then sieved in both containers at time $t = 0$ hours while ambient temperature was of $-10\,^{\circ}\mathrm{C}$. A 45 cm diameter sifter was employed with a mesh size of 4 by 6 mm. Prior to sieving, a 5 mm ice layer was applied to the bottom copper plate by spraying cold water with a spray bottle.

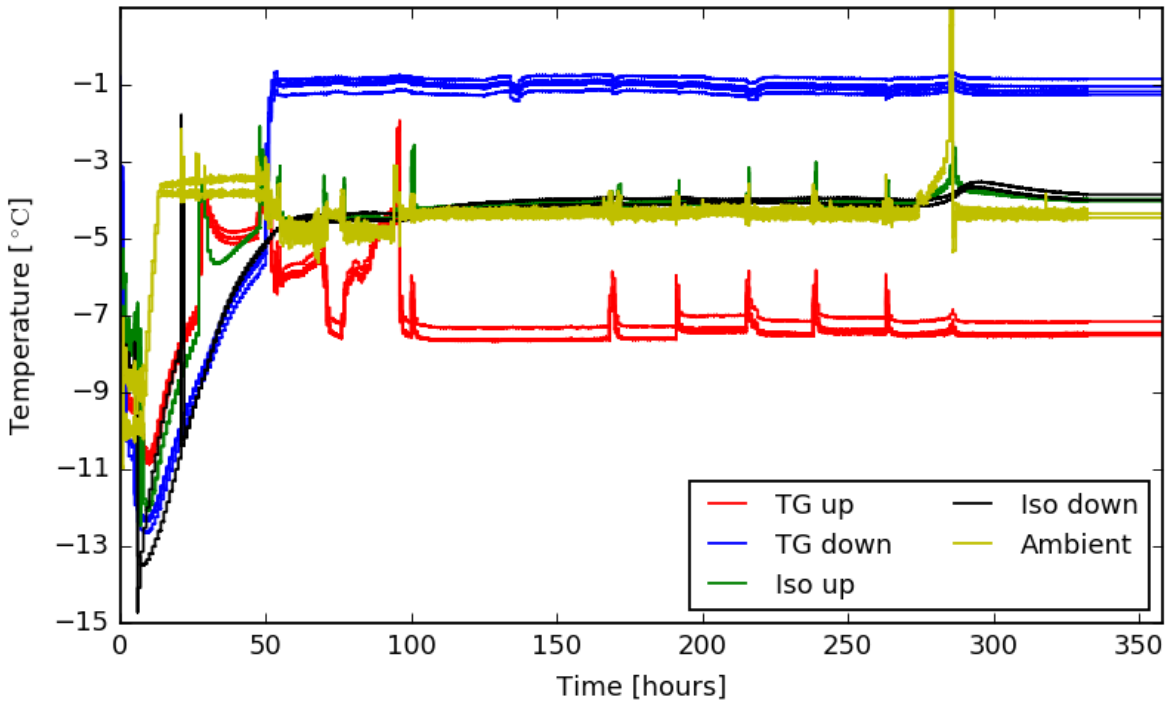

Figure 3: Temperature curves for upper and lower surfaces of apparatus as well as ambient temperature in the cold room.

2.3 Measurements

A first SMP measurement is performed one hour after sieving. Samples are then left to sinter for 40 hours, while ambient temperature reaches $-4\,°C$. After 40 hours' time, the effects of sintering on snow cohesion will be disregarded and only gradient metamorphism will be considered. Afterwards, measurements are performed on a daily basis during 15 days (360 hours). Monitored temperatures of samples and ambient temperatures are shown on Figure 3.

A measurement is performed at time t on its dedicated measurement zone. Measurement zone layout is shown on Figure 4a. In a single zone are conducted three SMP measurements, four vertical density measurements, three vertical SSA measurements and a qualitative evaluation of snow grains with a microscope. Minimal spacing between SMP measurements is of 8 cm and is assumed sufficient according to experimental results from [Herwijnen, 2013]. Density and SSA is evaluated vertically (Figure 4b) in order to assess effects of depth. Moreover, a global density (for the entire snow sample) will be computed knowing the dimensions of the sample and assuming constant mass. The width and length of the sample are constant throughout the experiment and obtained approximately by measuring the sample whereas the height variations are picked up from the SMP signal. SMP probing is done from above as the device is installed on a table overhanging the snow sample as shown in Figure 5b. SMP probing is always performed prior to density and SSA measurements to ensure the integrity of the snow sample. Density is measured with a snow cutter of following dimensions: 2.47 x

9.80 x 10.30 = 248.1 cm^3 and SSA is measured with DUFFFIS [Gallet et al., 2009].

3 Analysis Method

3.1 Shot Noise

Löwe and van Herwijnen [2011] derived the following micro structural parameters from statistical characteristics of the SMP force signal:

$$f_0 = \frac{3}{2}\frac{\kappa_2}{\kappa_1}, \qquad \delta = -\frac{3}{2}\frac{C(0)}{C'(0)}, \qquad \lambda\delta = \frac{4}{3}\frac{\kappa_1^2}{\kappa_2}, \tag{1}$$

where f_0, the micro structural force, depends of both first and second cumulants κ_1 and κ_2 of the shot noise process, respectively the mean and the variance of the force signal on a given window. Then, δ is the micro structural deflection at rupture of an element and depends upon the covariance C of the signal at its origin. Finally, λ is the number of occurring ruptures per mm (traveled by the SMP rod) in the vicinity of the cone surface.

This model was further modified: parameters (3) are computed from a stationary signal (2) and variations of λ with depth are taken into account. This method yields better results when compared to synthetic signals as it is assumed to better include the effects of the development of a compaction zone around the cone as probing begins.

$$\tilde{F} = \frac{F - \overline{F}}{\overline{F}^{1/2}} \tag{2}$$

$$f_0 = \frac{3}{2}\left\langle \tilde{F}^2 \right\rangle, \qquad \delta = -\frac{3}{2}\frac{C(0)}{C'(0)}, \qquad \lambda = \frac{4}{3\delta}\frac{\overline{F}}{\langle \tilde{F}^2 \rangle} \tag{3}$$

In this study we will use this modified version of the shot noise model called non-homogeneous Poisson process (NHPP) due to a non-constant λ with depth. The mean of the force to calculate the stationary signal $\overline{F}$ is calculated with a moving average of a window size of 5 mm. The microstructural parameters f_0 and δ were calculated over a window height of $\approx$ 30 mm and were assumed constant over this window.

3.2 Cavity Expansion Model

Based on Bishop et al. [1945]'s work on indenation theory of ductile materials with conical punches, Ruiz et al. [2017] derive from the equilibrium equation (4) a rate-dependent radial stress equation (5) which depends on bulk mechanical properties of snow. In the latter, r is the radius of the cavity, r_c is the cone radius and ν is Poisson's coefficient in snow (≈ 0.22).

$$\frac{\partial \sigma_r}{\partial r} = -\frac{\sigma_r - \sigma_\theta}{r} \tag{4}$$

$$\sigma_r(r) = \frac{\sigma_{mac}}{\sqrt{3}}\left(1 + \ln\left(\frac{\sqrt{3}E_{mac}}{2(1+\nu)\sigma_{mac}}\right) - 2\ln\left(\frac{r}{r_c}\right)\right) \tag{5}$$

Equation (5) is summed on the entire cone surface to yield the radial force:

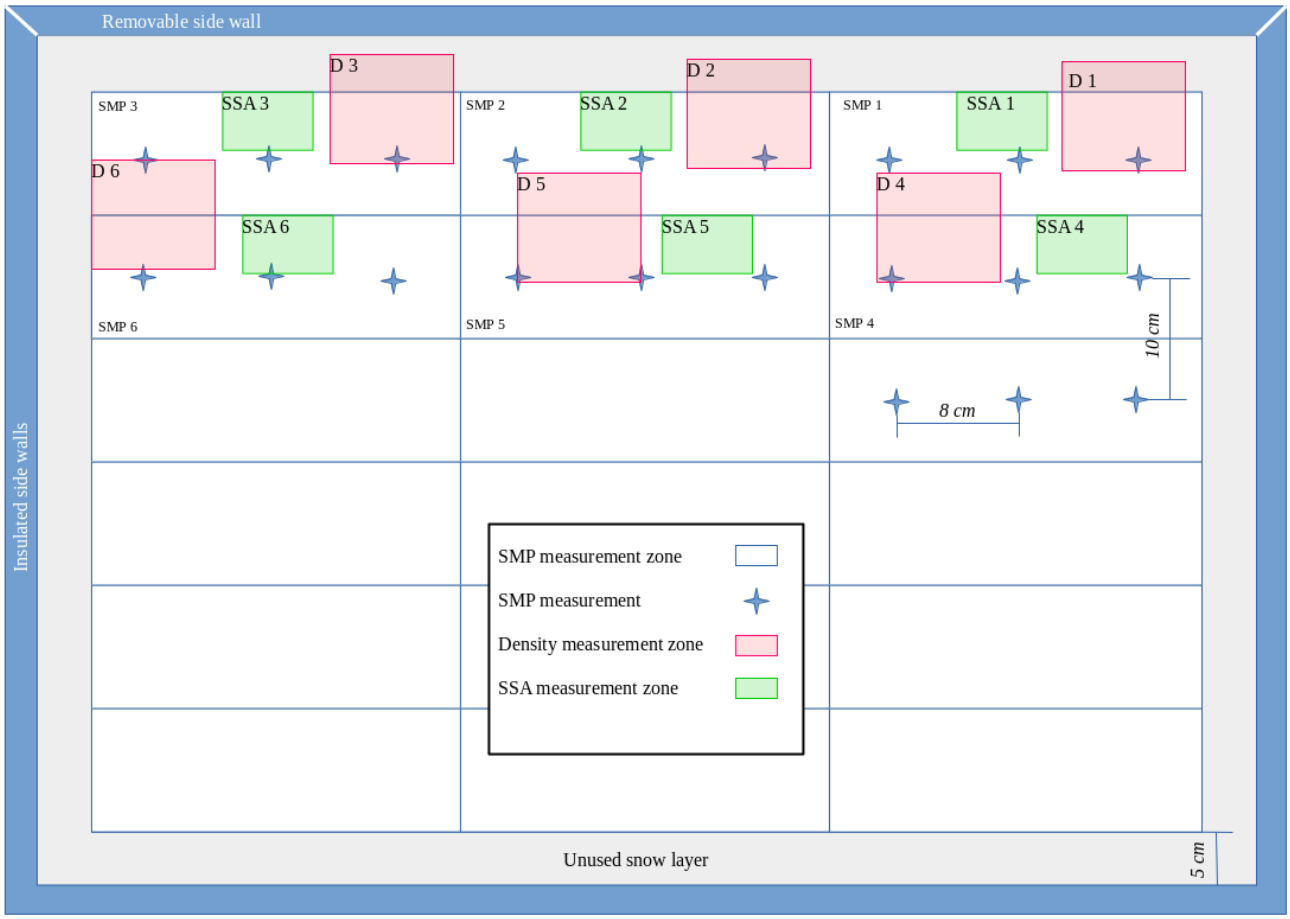

(a) Top view

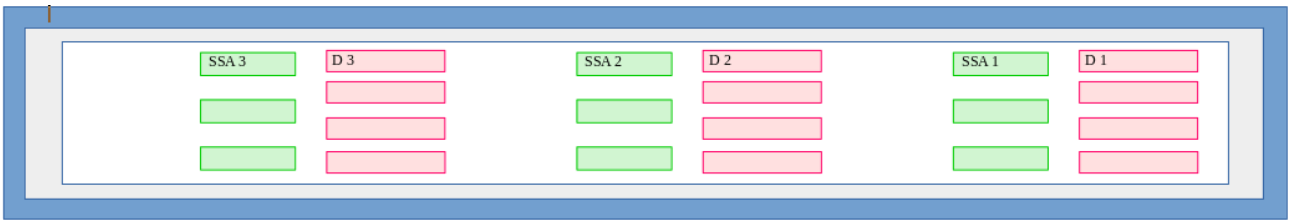

(b) Front view

Figure 4: Approximate measurement layout for both temperature gradient and isothermal apparatus.

(a) Temperature gradient apparatus with side wall and upper plate removed to measure density gradient and SSA.

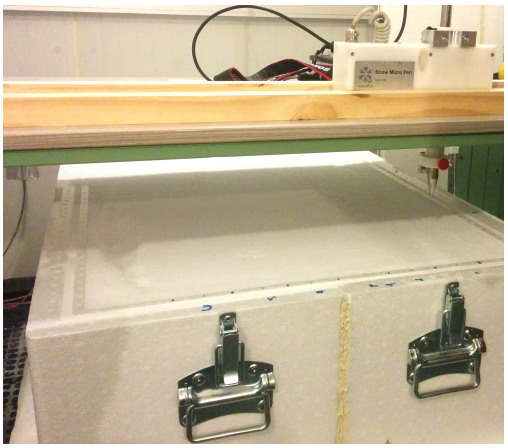

(b) Isothermal apparatus seen from above, about to perform SMP measurement.

Figure 5: Performing density, SSA and SMP measurements.

$$F_r = 2\pi \cot(\alpha) \int_0^{r_c} \sigma_r(r) r dr. \tag{6}$$

Then the vertical component of F is calculated, knowing the semiapex angle of the cone $\alpha = 30\,°$:

$$F_z = F_r \tan(\alpha). \tag{7}$$

Finally, F_p is the total vertical force acting of the cone taking into account the frictional force. The coefficient of friction of snow on steel used is of $\mu \approx 0.5$.

$$F_p = F_z(1 + \mu \cot(\alpha)) \tag{8}$$

This model is implemented by computing σ_{mac} and E_{mac} over a moving window sweeping a single SMP force signal. Then σ_{mac} and E_{mac} are obtained by minimizing the least square differences between the SMP force signal and F_p.

3.3 Density

In addition to the measured density, we compute a density from Proksch et al. [2015]'s model based on the force signal's median $\bar{F}$ and mean structural element length L:

$$\rho_{Pr} = a_1 + a_2 \ln \bar{F} + a_3 \ln(\bar{F}) L + a_4 L \tag{9}$$

where parameters a_i are calibrated by minimizing the square differences with density experimental data obtained with the density cutter over all signals of both snow samples. Optimization is done using 4 windows per signal to comply with cutter data. Mean structural element length is $L = \left(\frac{A}{\lambda}\right)^{\frac{1}{3}}$ where λ is the shot noise parameter which consists in the

number of ruptured elements per mm computed from the SMP's force signal and A is the projected cone surface.

Another density is computed, the sample's global density, where mass, width and depth are assumed constant therefore only height variations of the sample are considered and are best fit to density cutter data by finding the initial value (ρ at t=0) of density which minimizes the squared differences.

4 Results

4.1 Density and SSA

Samples are initially similar, their global mean density increase are also alike. However, density cutter values of the TG sample show greater variations with depth (stratification). Proksch's model features a less steep slope than the cutter values.

SSA's are initially alike for both samples and decrease with time. Towards the end the TG sample reaches lower values. No significant stratification is observed.

4.2 Force signals

Figures 7a and 7b feature force signals plotted against depth. The first SMP force signal, at $t = 0$ hours, is obtained right after sieving and hence has not yet undergone sintering. Moreover, the temperature gradient was only established after 40 hours. Thus we consider the experiment to have begun at $t = 40$.

This data is plotted differently in Figures 7c and 7d where stratification is now highlighted.

The isothermal sample shows a gradually increasing force through time that is more pronounced near the bottom of the snow sample. A gap is observable between 0 and 40 hours.

The TG sample features a less pronounced increase in force with depth. As for time dependence, it is strongly discontinuous from 94 to 162 hours where the force signal decreases abruptly and then increases slightly to reach a stable state around 238 hours.

Comparison between both samples show similar initial states but diverging behaviors as time goes by. The isothermal snow shows twice the average penetration resistance at the end of the experiment compared to TG snow.

4.3 Poisson shot noise parameters

Figures 8 and 9 show the shot noise model's three microstructural parameters. Once again, data is plotted in two different fashions, in Figure 8 parameters are plotted against depth on the y-axis whereas Figure 9 highlights the time-evolution of the parameters.

The isothermal sample shows, with time, a constant δ, an increasing f_0 and slight decrease in λ. Stratification is observed only for f_0 which increases in the lower layer of the sample but remains constant in the upper layer.

The gradient sample features, with time, an increase of δ and f_0 but a decrease of λ. Stratification is seen in both δ and f_0.

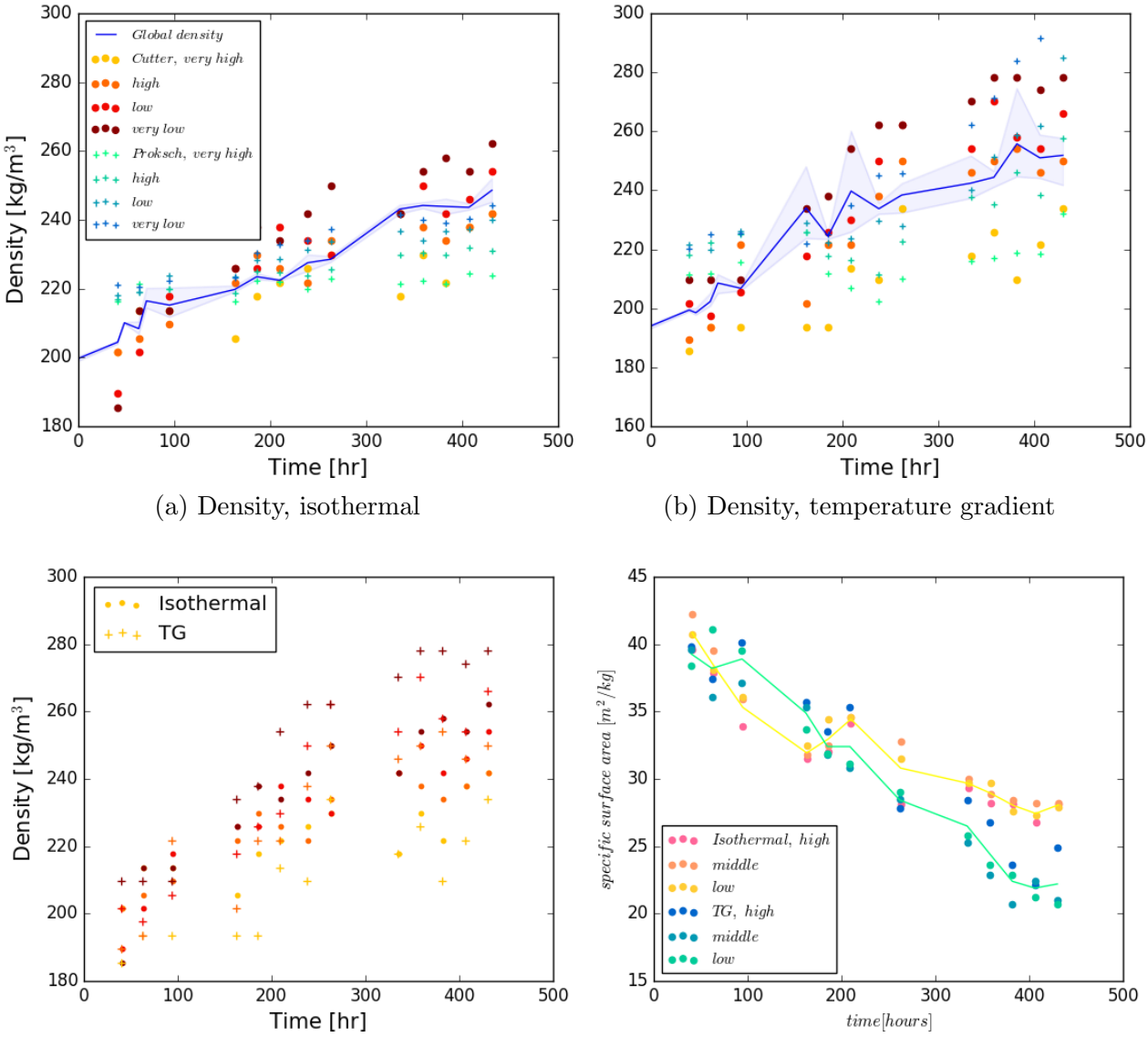

(a) Density, isothermal

(b) Density, temperature gradient

(c) density cutter data for both samples

(d) Specific surface area for both samples.

Figure 6: (a,b) Evolution of density through time for both snow samples. Global density is calculated from the height of the snow sample which was retrieved from the SMP signal. Density from cutter is plotted according to its vertical position on the cross-section of snow sample (see Figure 4b). Proksch's model is also plotted after calibration with cutter data. (c) Cutter data for both samples are then plotted together to highlight difference in stratification. (d) Evolution of SSA through time for both snow samples measured with DUFISSS is also plotted where solid lines are the average and the dots are the layers.

4.4 Cavity Expansion Model

The CEM results in a small increase of bulk elastic modulus for isothermal snow and a significant increase for gradient snow. As for yield stress, the resulting signals have the same shape as the force signals.

The absolute values computed by the continuum cavity expansion model are dependent of the seed passed on to the minimization algorithm and hence can not be relied upon. This is due to the model being insufficiently constrained and possessing multiple local minima. The plotted results in Figures 11a and 11b were computed with seeds of $E_{mac} = 10^6$ Pa and $\sigma_{mac} = 10^4$ Pa obtained from Mellor [1974] for a density of 250 kg/m^3. However we can discuss the relative differences between signals.

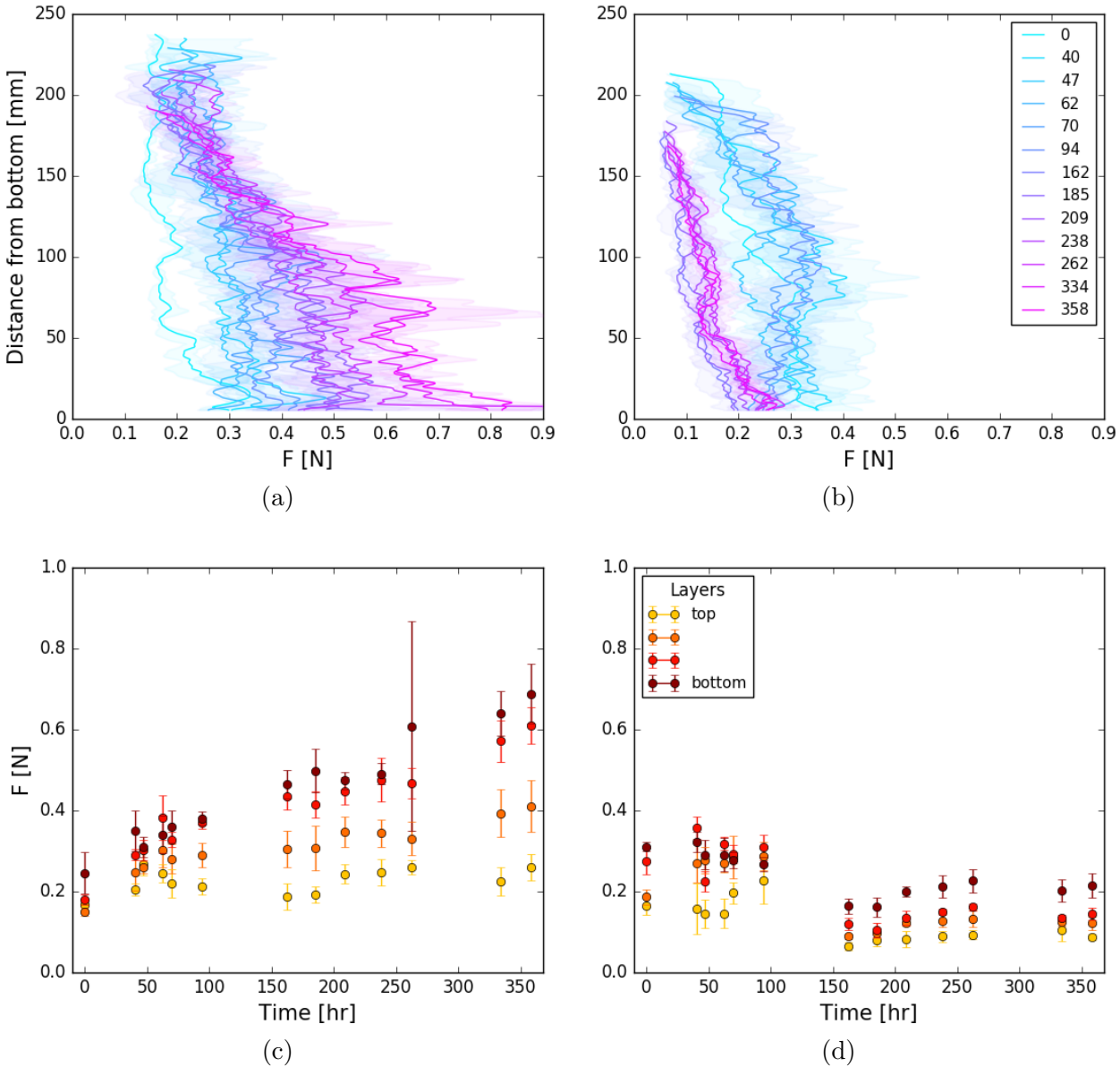

Figure 7: Evolution of SMP force signal through time (in *hours*) for both snow samples. Isothermal sample is on the left while gradient sample is on the right. (a,b) Data plotted against depth : curves are the mean values of three signals while filling shows their minima and maxima. (c,d) Data plotted against time : a point is the average of 6 values and the error bar is the standard deviation.

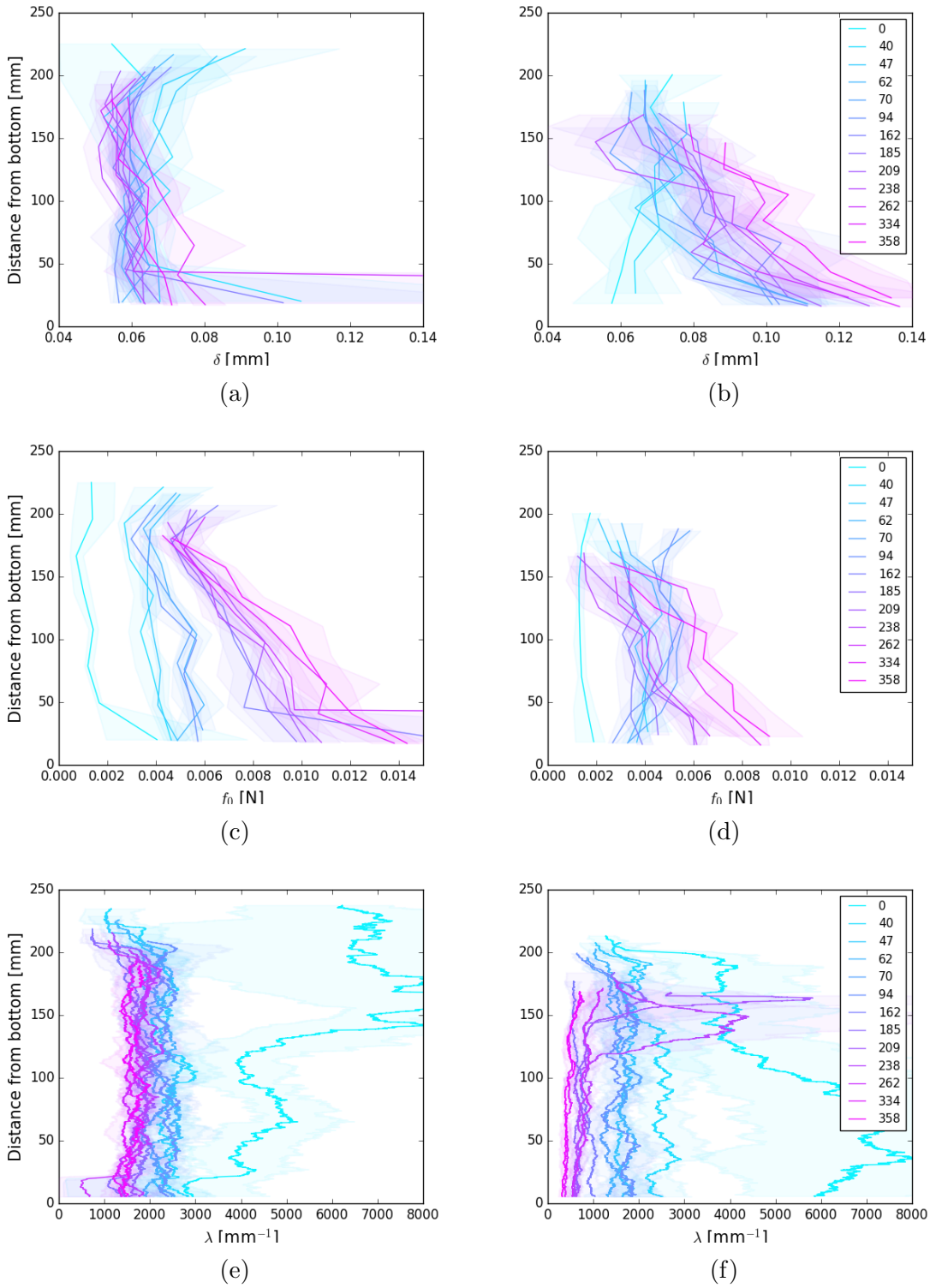

Figure 8: Evolution of microstructural parameters δ (a,b), f_0 (c,d) and λ (e,f) for both samples. Isothermal is plotted on the left and gradient is on the right.

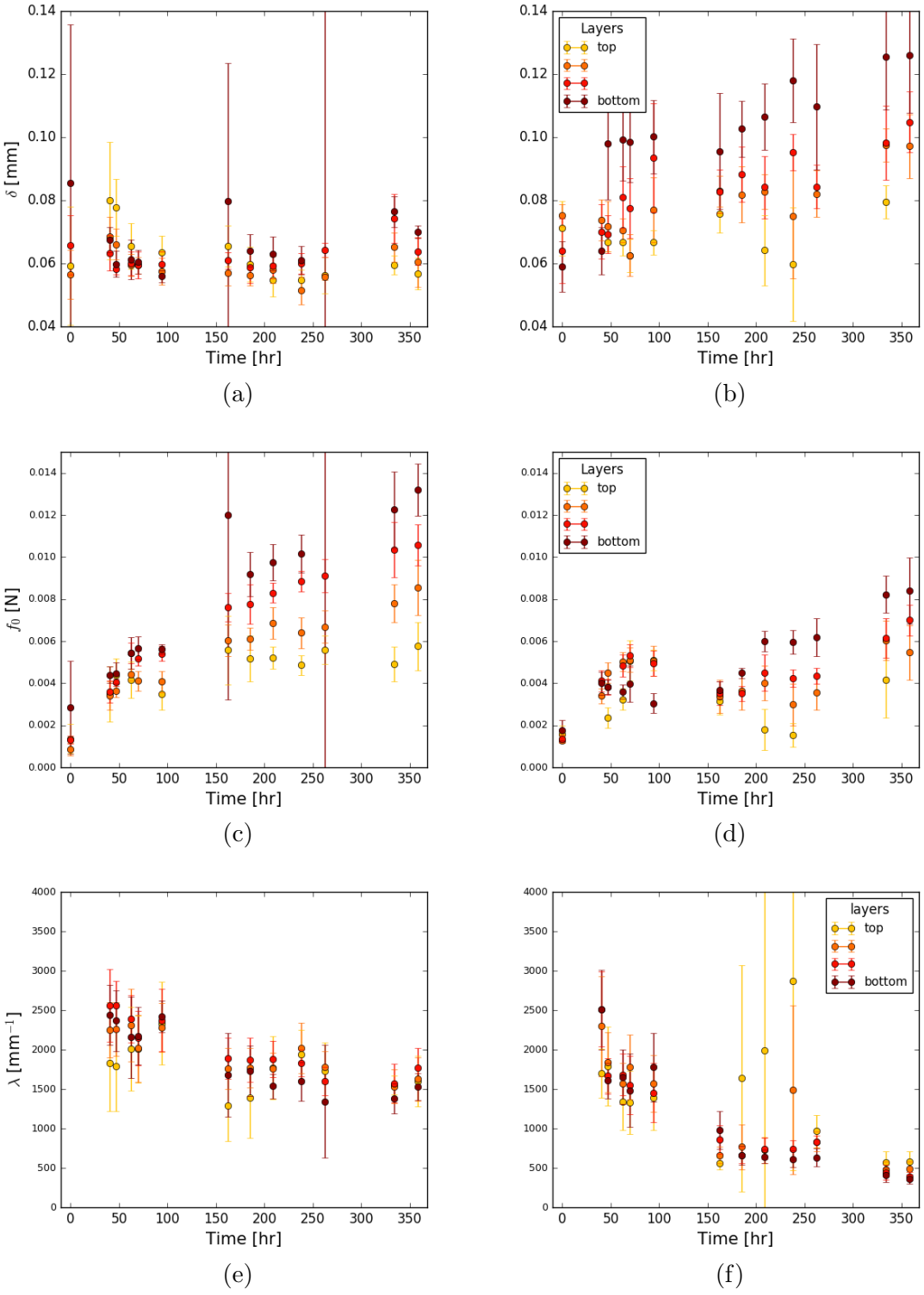

Figure 9: Evolution of microstructural parameters through time plotted differently to highlight change with time. Isothermal is on the left and gradient is on the right. Signals were condensed into 4 layers to ease readability. Thus each data point contains averaged values of 3 signals and 2 layers yielding 6 values. Error bars are the standard deviations and markers are the averages.

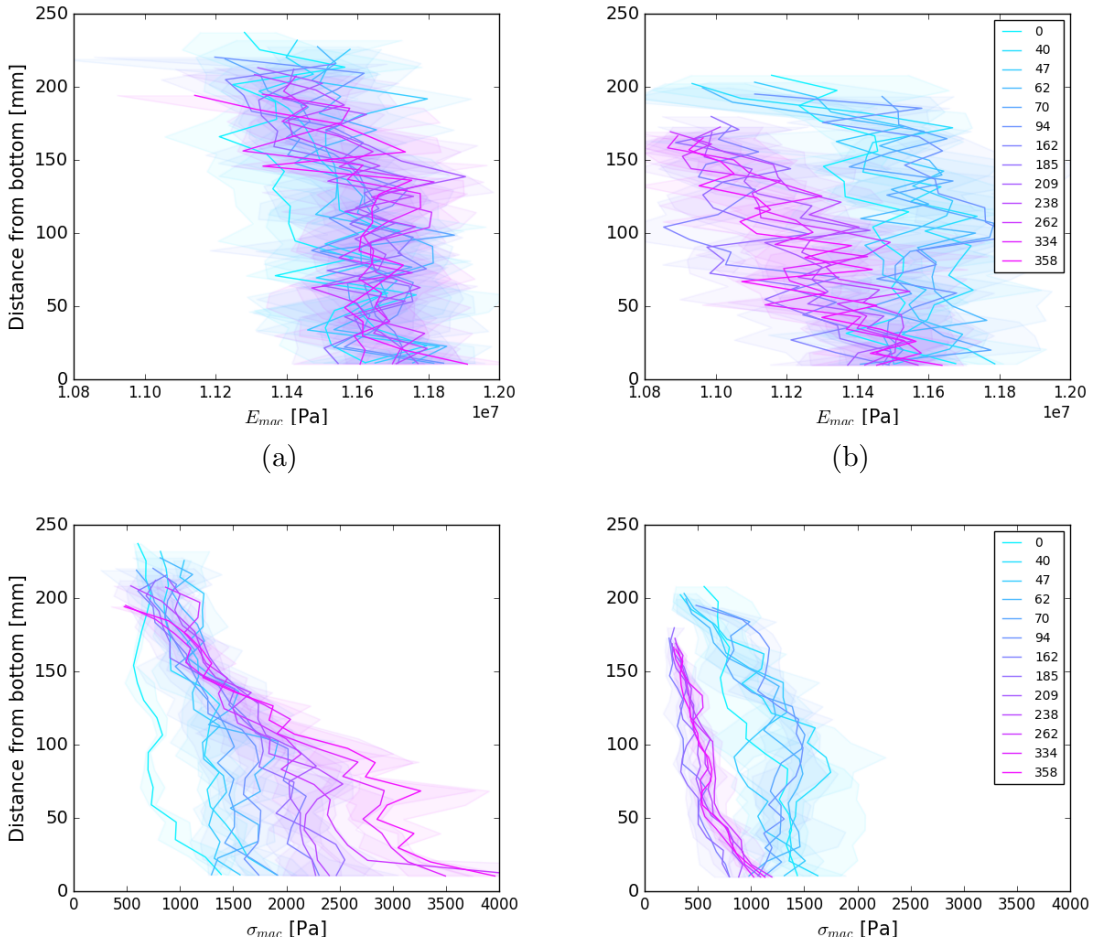

Figure 10: Evolution of E_{mac}, bulk elastic modulus, and σ_{mac}, yield stress, plotted against depth.

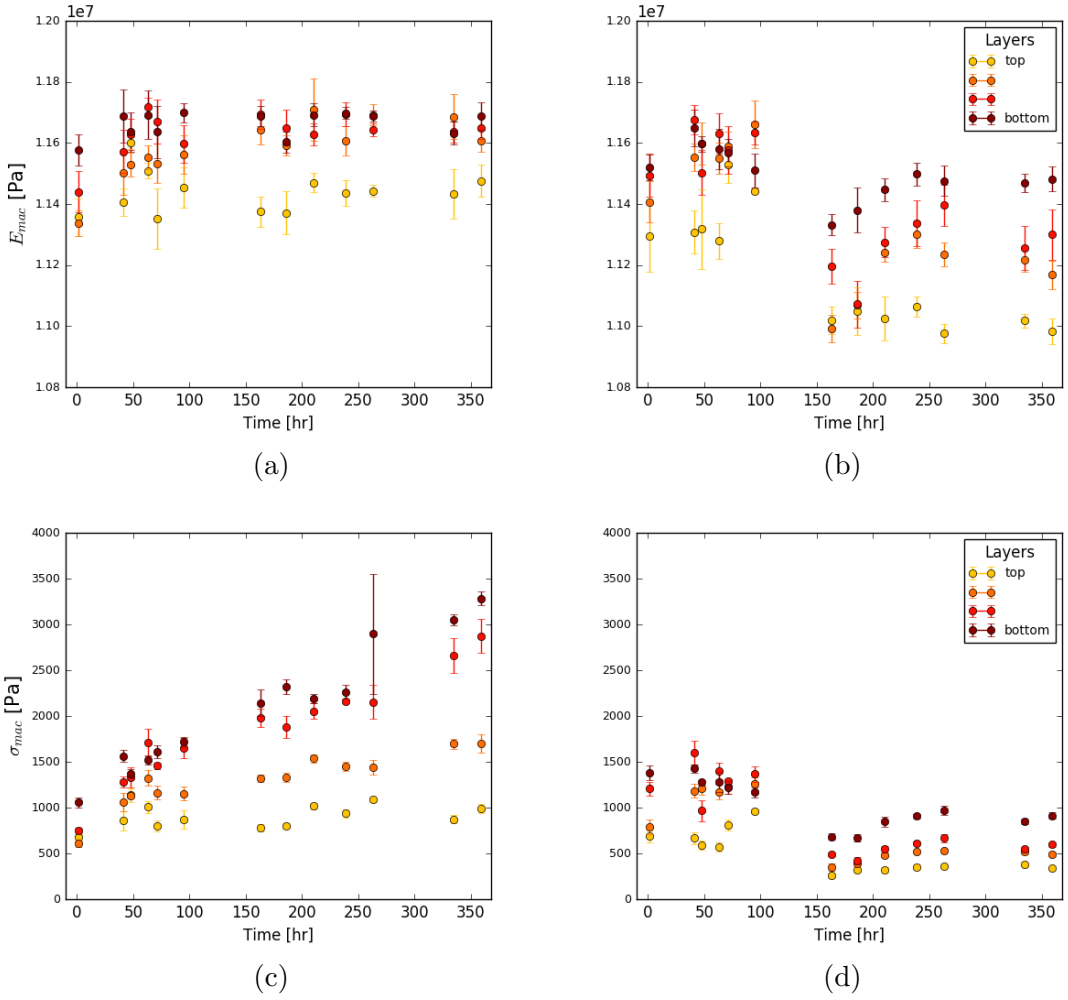

Figure 11: Evolution of E_{mac}, bulk elastic modulus, and σ_{mac}, yield stress, through time for both snow samples now plotted to highlight changes through time.

5 Discussion and Conclusion

5.1 Density and SSA

Density behaves similarly for both samples yet gradient snow shows greater stratification as indicated by the warm colored scatters on Figures 6a and 6b. On Figure 6c, we see that the lower layer of the gradient sample is denser than that of the isothermal sample. This can be caused by the proximity of the warm copper plate, as we know that warmer ice has lower viscosity and hence will undergo greater creep strain [Mellor, 1974].

Global densities are alike for both samples meaning that the heights of the samples matched during the entire experience. Experimental density curves feature slopes that are greater than that of Proksch's model. Indeed the model's trend resembles the average of both samples, certainly because it was calibrated on both samples. We conclude that it poorly predicts density through time for snow undergoing metamorphism.

SSA for gradient snow is similar to that seen in literature but differ slightly from Calonne et al. [2014]'s results due to different snow types. In our study we had an initial snow type of PP/DF whereas Calonne et al. [2014] had rounded grains, justifying our greater initial values of SSA. As for the final values, since our experiment did not yield fully developed cup-shaped grains due to insufficient time, we have higher values of SSA.

Our final values of SSA for isothermal snow coincide with that of rounded grains observed in literature.

5.2 Poisson shot noise

The isothermal sample features more or less constant values of δ and λ across its depth, yet f_0, the individual rupture force, increases (Figure 9). Thus, we can assume that the increase in F with depth, the total penetration resistance, is explained solely by this increase in f_0. In other words, the increase in penetration resistance with depth for the isothermal sample is not due to a greater number of ice bonds being ruptured (λ) but only to a strengthening of those bonds when approaching the bottom of the sample. Values of f_0 towards the bottom of the sample increase with time at rate twice as fast as values towards the top. This could be attributed to the effect of the stress from the weight of the upper layers of the sample. A greater stress will increase contact pressure between grains which can accelerate various sintering mechanisms [Flin, 2004].

The TG snow sample's F signal features a significant gap from 94 to 162 hours where it evolved drastically. Unfortunately the occurrence of this evolution coincided with a period where no measurements were performed, hence the strong discontinuity. At time $t = 162$ hours was also when were first observed facets on the grains (Figure 12). Thus the very beginning of faceting was not measured with the SMP.

The decreasing trend in F with time, from 162 hours and on, can be explained by a drop in λ. Indeed, it seems that the amount of ice bonds decreased to the benefit of either facet formation or that of other ice bonds. This trend is observed until the end of the experiment. Also, the strength of individual bonds f_0 rose with time, once again meaning that during strong-gradient metamorphism some ice bonds disappear while others gain in

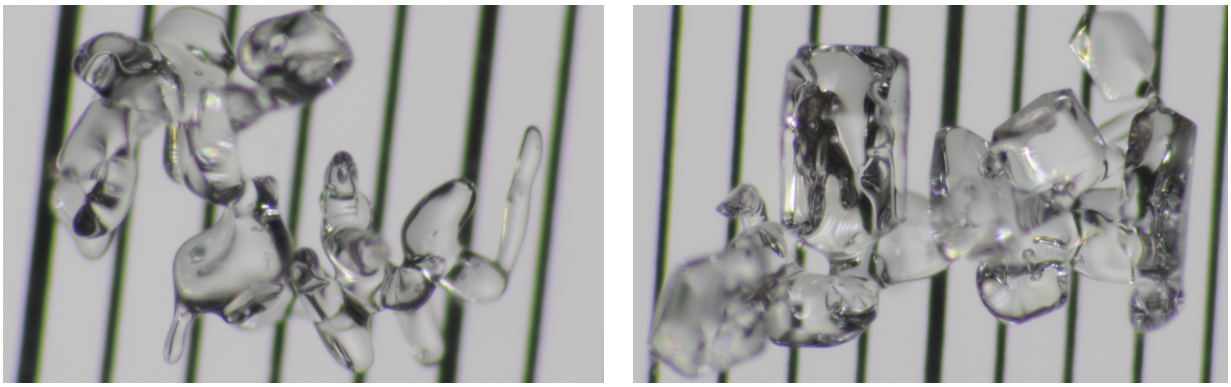

(a) Grain at t= 94 hours. (b) Grain at t= 162 hours.

Figure 12: Two different snow grains from TG sample between 94 and 162 hours for which period facets have formed. Scale of graduation is of 1 mm.

strength, yielding an overall decrease in cohesion and penetration resistance. As for the deflection at rupture δ, its increase is justified by a greater grain size due to faceting, which is visible through decreasing SSA. We can hypothesize that bigger grains, hence more distanced bonds, will rupture after greater deflection for an equal force applied.

The isothermal sample's SSA is also decreasing with time yet δ remains constant. Unlike the TG sample where grain growth lead to smaller SSA and greater deflection, the isothermal sample's decreasing SSA could be attributed to the snow grains attempting to reduce its surface energy, which implies also ice bond growth in both volume and strength, justifying also the rise of f_0.

To sum up, according to this microstructural model, faceted snow is less resistant to penetration due to a smaller number of ice bonds which are undergoing greater stress due to a lever-arm effect caused by grain growth. The ice bonds present amongst faceted snow are also growing and strengthening but at an insufficient rate to compensate for both aforesaid phenomena. As for rounded grains, their greater resistance is due to a more or less constant amount of ice bonds which are growing rapidly with time.

Several conclusions were drawn by observing the behavior in time and space of the microstructural parameters. Such conclusions could not have been drawn based solely on F, the penetration resistance signal. The Poisson shot noise model seems adequate to quantitatively characterize the evolution of snow with metamorphism and is able to reveal greater information on snow microstructure than would the force signal on its own.

5.3 CEM

The gradient sample shows a drop in modulus of elasticity (Figure 11b) as snow faceting begins. This is due to the fact that the vapor fluxes in snow undergoing gradient are mostly vertical [Calonne et al., 2014], reinforcing preferentially the bonds in a vertical fashion which leads to the formation of columns. Therefore the CEM, being a radial model, seems to have picked up this decreasing horizontal stiffness due to column formation.

However, the validity of the computed modulus of elasticity is doubtful as it should

increase greatly with density as seen in literature [Mellor, 1974], which is not observed here. No information is drawn from yield stress results.

References

M. Schneebeli and J.B. Johnson. A constant-speed penetrometer for high-resolution snow stratigraphy. *Ann. Glaciol*, 26:107–111, 1998.

C. Pielmeier and M. Schneebeli. Measuring snow profiles with high resolution: Interpretation of the force-distance signal from a snow penetrometer. Technical report, Swiss Federal Institute for Snow and Avalanche Research, Davos Dorf, Switzerland, 2003.

H. Löwe and A. van Herwijnen. A poisson shot noise model for micro-penetration of snow. *Cold Regions Science and Technology*, 2011.

S. Ruiz, A. Capelli, A. van Herwijnen, M. Schneebeli, and D. Or. Continuum cavity expansion and discrete micromechanical models for inferring macroscopic snow mechanical properties from cone penetration data. *Geophys. Res. Lett.*, 2017. doi: 10.1002/2017GL074063.

J. B. Johnson and M. Schneebeli. Characterizing the microstructural and micromechanical properties of snow. Technical report, Swiss Federal Institute for Snow and Avalanche Research and U.S. Army cold regions reasearch and engineering laboratory, 1999.

H.-P. Marshall and J. B. Johnson. Accurate inversion of high-resolution snow penetrometer signals for microstructural and micromechanical properties. *J. Geophys. Res.*, 114, 2009. F04016.

M. Mellor. A review of basic snow mechanics. Technical report, U.S. Army cold region research and engineering laboratory, Hanover, NH, 1974.

M. Proksch, H. Löwe, and M. Schneebeli. Density, specific surface area, and correlation length of snow measured by high-resolution penetrometry. *J. Geophys. Res. Earth Surf.*, 120:346–362, 2015. doi:10.1002/2014JF003266.

N. Calonne, F. Flin, C. Geindreau, B. Lesaffre, and S. Rolland du Roscoat. Study of a temperature gradient metamorphism of snow from 3-d images: time evolution of microstructures, physical properties and their associated anisotropy. *The Cryosphere*, 8:2255–2274, December 2014.

C. Fierz, R.L. Armstrong, Y. Durand, P. Etchevers, E. Greene, D.M. McClung, K. Nishimura, P.K. Satyawali, and S.A. Sokratov. *The International Classification for Seasonal Snow on the Ground*. UNESCO-IHP, Paris, ihp-vii technical documents in hydrology no 83 edition, 2009.

A. V. Herwijnen. Experimental analysis of snow micropenetrometer (smp) cone penetration in homogeneous snow layers. *Can. Geotech. J.*, 50:1044–1054, 2013.

J.-C. Gallet, F. Domine, C. S. Zender, and G. Picard. Measurement of the specific surface area of snow using infrared reflectance in an integrating sphere at 1310 and 1550 nm. *The Cryosphere*, 3:167–182, 2009.

R. F. Bishop, R. Hill, and N.F. Mott. The theory of indentation and hardness tests. In *The proceedings of the physical society*, volume 57, 1945.

F. Flin. *Description physique des mtamorphoses de la neige partir d'images de microstrucutres 3D naturelles obtenues par microtomographie X*. PhD thesis, Universit Joseph Fourier, Grenoble, 2004.